Crossed-Nanowire Molecular Junctions: A New Multispectroscopy Platform for Conduction-Structure Correlations

ARTICLE *in* NANO LETTERS · AUGUST 2010

Impact Factor: 13.59 · DOI: 10.1021/nl100982q · Source: PubMed

6 AUTHORS, INCLUDING:

Heayoung P. Yoon
National Institute of Standards and Techn…
20 PUBLICATIONS **398** CITATIONS
SEE PROFILE

Masato M Maitani
Tokyo Institute of Technology
37 PUBLICATIONS **344** CITATIONS
SEE PROFILE

T.s. Mayer
Pennsylvania State University
205 PUBLICATIONS **4,540** CITATIONS
SEE PROFILE

David L Allara
Pennsylvania State University
261 PUBLICATIONS **23,054** CITATIONS
SEE PROFILE

NANO LETTERS

pubs.acs.org/NanoLett

Crossed-Nanowire Molecular Junctions: A New Multispectroscopy Platform for Conduction−Structure Correlations

Heayoung P. Yoon,[†] Masato M. Maitani,[‡] Orlando M. Cabarcos,[§] Lintao Cai,[†] Theresa S. Mayer,*[,†,‡] and David L. Allara*[,‡,§]

[†]Department of Electrical Engineering, [‡]Department of Materials Science and Engineering, and [§]Department of Chemistry, The Pennsylvania State University, University Park, Pennsylvania 16802

ABSTRACT We report a crossed-nanowire molecular junction array platform that enables direct measurement of current−voltage−temperature characteristics simultaneously with inelastic electron tunneling and Raman vibrational spectra on the same junction. Measurements on dithiol-terminated oligo(phenylene-ethynylene) junctions show both spectroscopies interrogate the gap-confined molecules to reveal distinct molecular features. This versatile platform allows investigation of advanced phenomena such as molecular switching and cooperative effects with the flexible ability to scale both the junction geometries and array sizes.

KEYWORDS Self-assembled monolayer, nanowire, inelastic electron tunneling spectroscopy, surface enhanced Raman spectroscopy, molecular conduction, molecular electronics

Electronic devices fabricated from junctions with bridging self-assembled molecular monolayers (SAMs) offer unparalleled design flexibility and scalability not found in inorganic material systems. The major focus of research in this area has been on metal−molecule−metal (M^3) junctions, and a variety of studies have shown that through proper design and selection of the molecular structure, end groups, and metal contacts, important operational functions can result, including negative differential resistance, bistable switching, and chemical transduction.[1−5] Underlying successful use of such functions is the need to definitively understand the charge transport mechanisms and the dynamic correlations with molecular structure under conditions of active junction bias. Recent work, however, has shown that the conduction properties of these junctions can be strongly influenced by variations in the molecular geometry and contact bonding, which in turn depend on the precise makeup of the fabricated junction.[6−8] This has made it difficult to extract fundamental molecular design parameters without a corresponding understanding of the geometrical and chemical structure of the junction.

Combining electrical and in situ spectroscopic characterization techniques provides an ideal strategy to extract molecular structure−conduction correlations on the same molecular junction. When obtained from reproducible solid state molecular junctions, such data can provide critical information needed for developing cohesive theories to predict molecular transport, including conduction mechanisms and dissipation characteristics. Options for in situ spectroscopic probes in the highly confined, nanoscale geometries of these junctions are severely limited to those that depend selectively upon intrinsic features of the junctions, namely, charge transport and the nanoscale gap. Two powerful spectroscopy techniques that can fit within these limitations are inelastic electron tunneling spectroscopy (IETS) and surface-enhanced Raman spectroscopy (SERS). Both of these probes provide information on vibrational transitions of the molecules in the junction which in turn can reveal incisive information on molecular structure.

IETS can be obtained directly from the second harmonic signal ($\sim d^2I/dV^2$) in a current−voltage ($I-V$) measurement at low temperature (<10 K). The spectra provide both dipole and induced dipole allowed transitions of the molecules participating in charge transport and have been interpreted to give valuable information on bonding geometry,[9] transport pathways,[10] and in situ interaction to the tunneling electrons in the nonequilibrium state.[11] IETS alone, however, is limited in revealing critical information because of the common issues of spectral complexity (e.g., phonon coupling, junction orientation)[12] that requires significant theory effort for interpretation and insufficient energy resolution relative to typical molecular line widths in small ensembles.

SERS, via laser excited electromagnetic surface plasmon polariton (SPP) coupling with metal and molecule electrons in an open nanoscale junction gap, offers a highly useful complement to IETS by providing an independent probe at induced dipole transitions with the added advantage of spectral resolutions 10^2 times greater than for typical IETS. The sensitivity of SERS for confined molecules within an appropriate nanoscale metal gap can approach the single molecule level at room temperature.[13,14] In addition, a recent study has demonstrated the utility of SERS in direct

* Corresponding authors, tsm2@psu.edu and dla3@psu.edu.
Received for review: 03/19/2010
Published on Web: 07/13/2010

DOI: 10.1021/nl100982q | *Nano Lett.* **2010,** *10,* 2897–2902

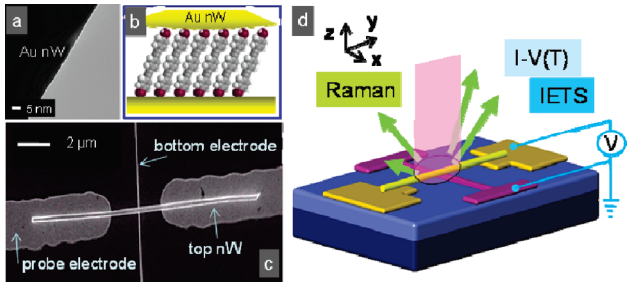

FIGURE 1. (a) Transmission electron microscope image of a template-grown 220 nm diameter Au nW. The atomically flat surface of the nW was used as a top contact to a 60 nm wide lithographically patterned bottom Au contact in the X-nWJ. (b) Schematic of the OPE SAM embedded between the crossed-area of the top and bottom Au contacts to give an electrically contacted 2 nm thick molecular layer. (c) Field emission scanning electron microscope (FESEM) image showing the fabricated junction. (d) Schematic of the electrical and multispectroscopic measurements that are made on the X-nWJ platform.

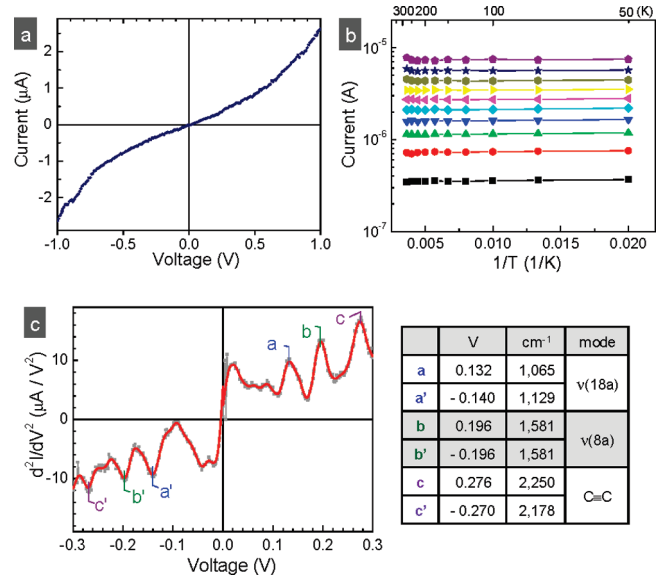

	V	cm⁻¹	mode
a	0.132	1,065	ν(18a)
a'	- 0.140	1,129	
b	0.196	1,581	ν(8a)
b'	- 0.196	1,581	
c	0.276	2,250	C≡C
c'	- 0.270	2,178	

FIGURE 2. Current−voltage data for representative X-nWJs. (a) A $I-V$ sweep from 0 to ±1 V at 300 K on an OPE X-nWJ shows a typical nonlinear characteristic. (b) Temperature-independent Arrhenius behavior for a series of different applied biases (0.1−1 V in steps of 0.1 V) rules out process-induced impurity conduction in the junction. (c) A typical IET spectrum obtained at a substrate temperature of 4.2 K with an ac modulation voltage of 6 mV (0 to ±0.3 V steps in 2 mV increments) at a frequency of 433 Hz. The measured data and the five-point smoothed fit are plotted using a solid square/thin line (gray) and thick (red) line, respectively. The peaks identified by a (a′), b (b′), and c (c′) in positive (and negative) bias polarities are due to the ν(18a), ν(8a), and C≡C stretch vibrational modes of the OPE molecules.

observations of local heating effects during conduction in molecular junctions.[15,16] Thus, the use of IETS and SERS in parallel with temperature dependent $I-V$ measurements on the same junction can potentially provide an incisive means to probe the conduction−structure relationship of the electrically active molecules in the junction.

In this Letter, we report a versatile and highly scalable crossed-nanowire molecular junction (X-nWJ) device platform that allows a direct correlation between the junction conduction properties over a wide temperature range (4−300 K) and the molecular structure by IETS and SERS on the same junction. Arrays containing hundreds of nominally identical configured X-nWJ's that probe a SAM of oligo(phenylene-ethynylene) (OPE) dithiol molecules were fabricated by deterministic assembly of individual template-grown Au nanowires across lithographically defined Au nanowires. The temperature-independent conduction properties of these molecular junctions confirm that the dominant transport mechanism is coherent tunneling, while the in situ IETS and Raman provide mutually consistent vibrational mode features definitively in accordance with the structure of the OPE molecules, thereby confirming that the probes are providing structure diagnostics. These results demonstrate an experimental approach that can address and broadly correlate important phenomena such as local environment, collective effects, and intriguing bistable switching properties, with molecular structure and bonding.

The example of a X-nWJ device in Figure 1 consists of a separately synthesized 220 nm diameter Au nW (Figure 1b,d),[17] dielectrophoretically positioned across a fabricated 4 μm gap alignment/probe electrode[18,19] to contact an OPE dithiol SAM preassembled on a 60 nm wide vapor-deposited bottom electrode on an oxidized silicon substrate (Figures 1c,d). The highly flexible nanofabrication process allows wide variations in the diameters and types of nWs that can be integrated, with extensions to diverse materials including semiconductors, superconductors, and nanotubes. The integration of the X-nWJs is completed in parallel for approximately 100 pairs of alignment/probe electrodes (see Supporting Information), with over 50% yield of individual nW junctions (20−30% remaining with multiple nWs and 20−30% open), offering enough data for statistical analysis and, consequently, meaningful comparison between theory and experiment. Using a recent hybrid approach, higher assembly yields (>80%) can be achieved.[20]

For 140 devices fabricated in several independent runs, the majority (100) fell within the (median) current range of 500 nA to 5 μA at 1 V bias and showed a characteristic nonlinear current−voltage ($I-V$) curve (Figure 2a) at 300 K (see Supporting Information). For each set of temperature scan runs, junctions in this current range were selected (typically 2−4) at random for IETS scans and all these gave reproducible IET spectral features (Figure 2b). The junction to junction conductance variations for the majority of devices is expected on the basis of the bottom contact roughness (~1 nm root mean square by atomic force microscopy) while the outlying currents are likely due to defects intrinsic to the SAM junction fabrication.

The magnitude of the currents can be compared with our earlier data for a Au−(OPE SAM)−Pd end-on, in-wire junction carrying ~1.6 nA/molecule at 1 V[21] based on an average area of 0.21 nm^2 occupied by a single OPE molecule.[22] For an ideal X-nWJ with a 220 nm diameter nanowire cylinder

DOI: 10.1021/nl100982q | *Nano Lett.* **2010,** *10,* 2897--2902

contacting a 2 nm thick SAM on a 60 nm wide smooth, flat surface, the corresponding junction area from an elastic planar strain analysis[23,24] is ~700 nm^2, which leads to ~3.3 × 10^3 bridging molecules in full contact and a predicted current of ~5 μA at 1 V. This value is at the upper end of our typical data and shows the general agreement between measurements on different types of junctions, taking into account surface roughness (see Supporting Information).

The temperature independence of the $I-V$ response for junctions in the median range, illustrated in the Arrhenius plots in Figure 2b, shows a dominant coherent tunneling conduction mechanism is operating, consistent with our earlier work with in-wire junctions,[5] and further implying that the intrinsic molecular electronic properties are responsible for charge conduction, rather than mechanisms such as impurity-meditated transport or thermionic emission.[25]

Simultaneous IET spectra (d^2I/dV^2) were collected during the $I-V$ scans (Figure 2c)[26] at 4.2 K to minimize temperature broadening. The prominent peaks at 132, 196, and 279 meV arise from both dipole (IR) and induced dipole (Raman) allowed transitions and are assigned as primarily due to the ν(18a), ν(8a), and C≡C stretching modes, respectively, in agreement with reported IR, Raman and sum-frequency generation spectra of the pure molecule and SAM,[22,27] previous IETS data from a free-standing crossed-macro-wire device,[28] and density functional theory (DFT) calculations.[29] The symmetry of the peaks around zero bias is expected for the D_{2h} symmetry of the OPE molecule and confirms the origin of the spectrum from inelastic vibrational scattering within the molecule, thus confirming the integrity of the junction.

Raman spectra were obtained by focusing a 1 μm spot from a 632.8 nm HeNe laser onto the top of a junction by means of a confocal Raman microscope. Signals above the noise level only resulted when the laser was directly on the junction, as illustrated in Figure 3a (spot A, blue spectrum), establishing that only molecules located in the junction gap were observed and proving the spectrum arises via excited electromagnetic SPP coupling[30] with the metal and molecule electrons in the junction gap. Several junctions arbitrarily selected within the 500 nA to 5 μA current range (@1 V) were examined and all gave reproducible Raman spectra. The spectra are consistent with both previous spectroscopy studies[22,27] and our DFT calculations and further has the advantage of ~10^2 times the spectral resolution over IETS for detailed mode assignments. Moreover, the 633 nm excitation wavelength, far off the resonance Raman condition, establishes that intense SERS is possible for a wide variety of molecules with no specific electronic structure required. High signal-to-noise spectra (Figure 3a) can be obtained at low beam powers (0.3 mW) that avoid laser-induced degradation as shown in Figure 3b, consistent with the known ability of SERS under appropriate gap geometry to generate observable spectra down to the single molecule level.[31,15] Exposure at a 100 mV bias to low laser power (0.3 mW) produces no changes in the current, but at higher laser powers (~1 mW or higher), significant fluctuations in the spectra and current arise, indicative of photodamage (Figure 3b).

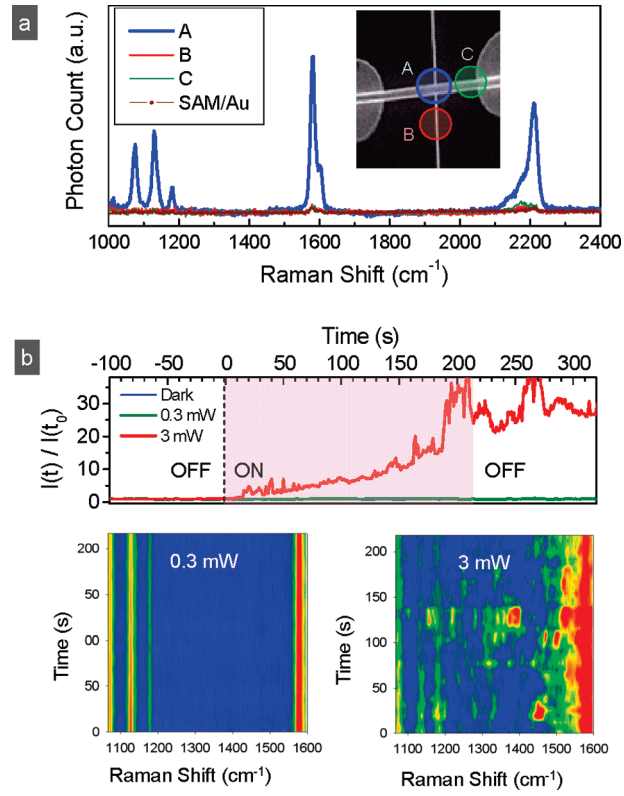

FIGURE 3. Raman spectra and electrical current under bias for OPE in a X-nWJ at room temperature. Raman spectra were obtained using HeNe laser excitation (0.3 mW or 3 mW, $\lambda = 633$ nm) with an acquisition time of ~50 s. (a) Laser irradiation over the sample junction results in observable spectra while positioning away from the junction gives no observable spectra. The line color corresponds to the position of the 1 μm diameter focused laser spot as denoted by the circles on the FESEM image. (b) In situ current versus time normalized to the current at $t = 0$ s, $I(t)/I(t_0)$. The junctions were measured at a bias of 100 mV in the dark (blue line) and at a laser power of 0.3 mW (green line) and 3 mW (red line) (top). Corresponding time-dependent Raman spectra are shown in the bottom panel. The current and Raman spectra are constant for junctions measured at a laser power of 0.3 mW, while both have significant fluctuations at 3 mW. Comparable $I(t)/I(t_0)$ were measured in the dark and under exposure of 0.3 mW, yet the current under exposure of 3 mW increased significantly and remained high after exposure.

The large intensity SERS signals are fully consistent with the location of the scattering molecules in the Au−SAM−Au junction as shown by finite element numerical simulations, based on Maxwell's equations, of the local electromagnetic (EM) field in the gap volume (Figure 4a; see Supporting Information). The squared total (components in all directions summed) electric field $|E(\mathbf{r},\omega_0)|^2 = E_0^2$ at position $\mathbf{r}$ and incident frequency ω_0, calculated for the device structure in Figure 1 (standard dielectric functions for Au and SAM at 633 nm), is plotted in Figure 4b. The outcoupled intensity at Raman frequency ω' is proportional to $E_0^2 \cdot |E(\mathbf{r},\omega')|^2$, but E_0^2

DOI: 10.1021/nl100982q | Nano Lett. 2010, 10, 2897–2902

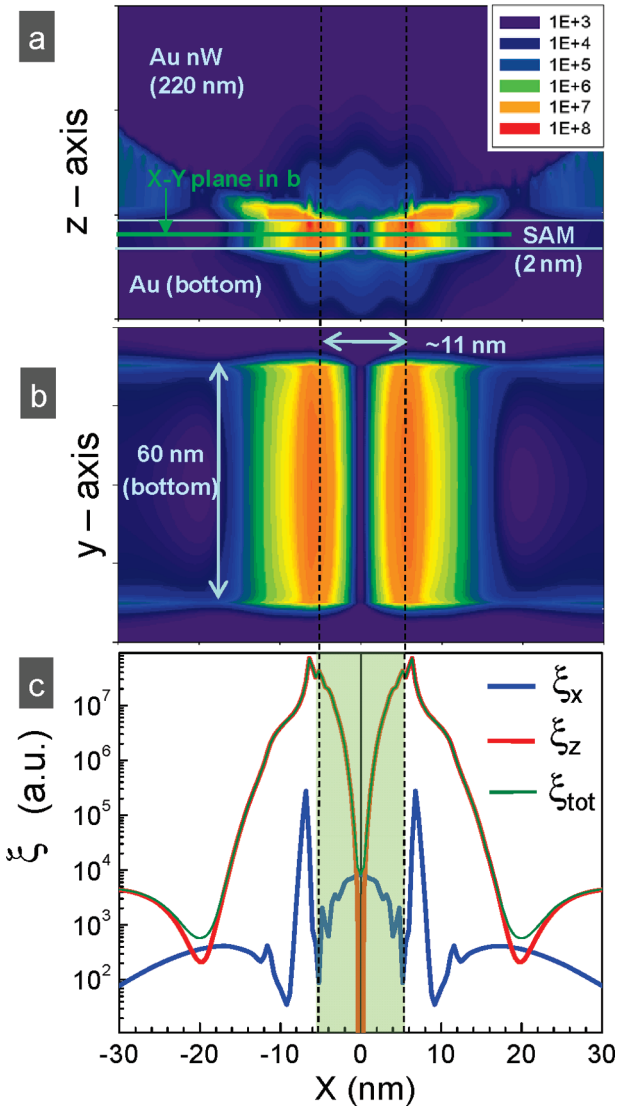

FIGURE 4. Total electric field $|E(\mathbf{r},\omega_0)|^2$, calculated from finite element electromagnetic field simulations, in the SAM between the top 220 nm diameter Au nanowire and bottom 60 nm wide Au contacts shown in (a) as a cross section through the center of the junction in the $x-z$ plane and in (b) as a top $x-y$ plan view through the center of the SAM layer. The local electric field was calculated relative to the incident excitation intensity (normalized electric field, 1 V/m; beam spot diameter on the bottom wire surface, 1 μm, λ = 633 nm). (c) Integrated electric field intensity per unit SAM thickness along the z axis of the SAM, $\xi = \int_{SAM}|E(\mathbf{r},\omega_0)|^2 dz/t_{SAM}$ for the x component (blue line), the z component (red line), and the total intensity (green line), where t_{SAM} is the SAM thickness. Note that ξ_y is vanishingly small on the scale of the plot. The $x-y-z$ coordinates for the junction are given in Figure 1d.

is plotted for simplicity. The calculation shows the dominant SERS excitation comes from the z-component of E_0^2 in the junction region (Figure 4a), thus favoring scattering via z-component elements of the polarizability tensor, which are manifested mainly along the long molecular axis thus opening the possibility of detailed molecular orientation analysis in the junction.

A simple analysis of the electromagnetic $E(\omega)$-field spatial distribution and charge conduction effects for chemisorbed OPE molecules shows that both SERS and $I-V$ signals are dominated by responses from roughly the same ensemble of bridging OPE molecules in the junction gap. First, integration of the $E(\omega)$-field over the junction region shows that ~50% of the incoming field is located in the gap region containing the bridging molecules. Combining the SERS intensity from this E-field with the extra SERS chemical enhancement factors of 10 to 100 for fully chemisorbed[32−34] thiol groups gives the prediction that >90% of the total SERS signal emanates from the fully bonded (Au−S−OPE−S−Au), bridging molecules in the gap region. Second, charge conduction is enhanced by more than a factor of ~5 for chemisorptive bridging at both ends of the OPE molecules, in comparison to single or double physisorption contact,[35,36] and tunneling through gaps between unbonded molecules and an electrode will reduce the conduction even further, thus leading to domination of conduction by Au−S−OPE−S−Au bridges. While this analysis establishes that SERS provides an incisive diagnostic of the device-active OPE molecules, more accurate calculations, and ideally low roughness junctions, will be required to quantitatively evaluate the limits of the correlation. Finally, also note the $E(\omega)$ calculations reveal that even large gap distances up to 10 nm can show significant SERS activity through the whole junction volume, thus potentially enabling measurements of large molecules (e.g., biomolecules), and the SERS intensity remains large across the 600−800 nm wavelength excitation range, allowing different excitation sources.

The excellent agreement between the information collected from the two spectroscopic probes is shown in Figure 5 where IETS data obtained at 4.2 K with a dc bias from 0 to 300 mV (2 mV increments in the sweep) are compared to Raman data collected at 300 K under a 100 mV dc bias (the current Raman microprobe setup does not allow cryogenic temperatures). The three main IETS peaks, ν_{18a} (1065 cm^{-1}, 132 mV), ν_{8a} (1581 cm^{-1}, 196 mV and $\nu_{C\equiv C}$ stretch 2226 cm^{-1}, 276 mV), match up extremely well with the Raman features at 1076.6 (133), 1135.3 (141), 1600.0 (198), and 2210.4 cm^{-1} (274 mV), respectively. In addition, the spectra show excellent agreement to a reported IETS theory prediction[29] as well as our DFT calculation of Raman and IR allowed transitions for an isolated molecule, establishing the integrity of the molecular structure of the bridging molecules. The overall comparison shows a distinct advantage of parallel IETS and Raman data as a strategy where peak matchup verifies that the same molecules are being interrogated by both techniques, thus justifying direct interpretations of different features in the two spectra to infer structures of the conducting molecules at chosen bias states.

In summary, we report a crossed-nanowire molecular junction fabricated by deterministic nanowire assembly that enables direct measurement of temperature-dependent $I-V$ characteristics in parallel with IET and Raman vibrational

DOI: 10.1021/nl100982q | *Nano Lett.* **2010,** *10,* 2897--2902

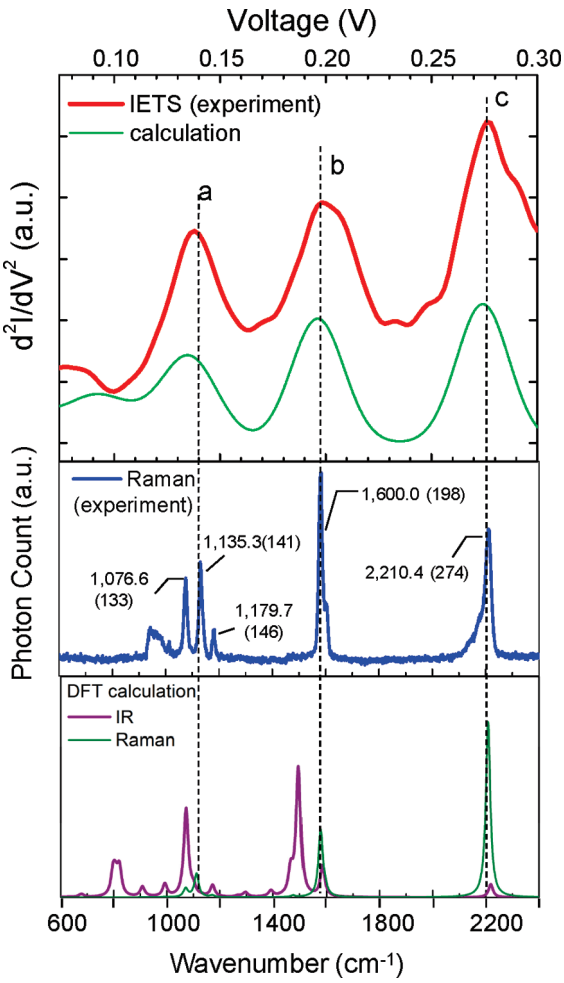

FIGURE 5. Comparison of the measured OPE IET (upper panel red line) and Raman spectra (middle panel) from a X-nWJ to the IETS theory (upper panel, green, which includes thermal broadening effects) and our DFT calculation of the Raman and IR of an isolated OPE molecule (lower panel, green for Raman, violet for IR). The IET spectrum was obtained at 4.2 K with an ac modulation of 6 mV, and the Raman data were collected at 300 K with a dc bias of 100 mV and a laser power of 0.3 mW by integrating the response over a 50 s exposure. The X-nWJ measurements are probing a few thousand OPE molecules between the top and bottom Au contacts. The three main peaks of a (ν_{18a}), b (ν_{8a}), and c ($\nu_{C\equiv C}$) were observed in both the IET and the Raman spectra and show an excellent matchup to the IETS theory prediction and our DFT calculation, which deliberately includes added line broadening (~20 cm^{-1} fwhm from a Voight type function) to the vibrational transitions for purposes of comparison to experiment.

spectra on the same junction. Measurements on dithiol-terminated OPE junctions show that the same conducting molecules are interrogated by each technique and that spectral features distinct to the molecular structure are easily resolved. These results demonstrate the versatility and high reproducibility of the X-nWJ device as a combined charge conduction and spectroscopic platform capable of ferreting out structure−conduction correlations over a wide range of temperatures and molecules, including mixtures in SAMs and potentially biomolecules, with junction dimensions scalable over orders of magnitude. Work is currently in progress in our laboratories to fabricate junctions with lower surface roughness bottom contacts, using methods such as directly placed single crystal nWs, with applications to studies with a variety of electronically active molecules and extensions to multiwavelength excited Raman, including anti-Stokes spectra, generated both in the incoherent[16] and nonlinear coherent modes.

Acknowledgment. The authors acknowledge financial support from DARPA/ONR and the NSF funded PSU Center for Nanoscale Science (MRSEC DMR-0080019), the use of facilities at the Penn State Site of the NSF NNIN under Agreement #0335765, and Ping Kao and Bangzhi Liu for experimental assistance.

Supporting Information Available. Details of nanowire and molecule synthesis, junction fabrication, alignment and probe electrode layout, *I*−*V* and Raman measurements, theory simulations, surface roughness of the thermally evaporated Au contacts, XPS characterization of OPE SAM, current−voltage properties of X-nWJs, Raman spectra of OPE, and EM field calculation of the X-nWJ structure. This material is available free of charge via the Internet at http://pubs.acs.org.

REFERENCES AND NOTES

(1) Heath, J. R. *Annu. Rev. Mater. Res.* **2009**, *39*, 1–23.
(2) Mantooth, B. A.; Weiss, P. S. *Proc. IEEE* **2003**, *91* (11), 1785–1802.
(3) Chen, J.; Reed, M. A.; Rawlett, A. M.; Tour, J. M. *Science* **1999**, *286* (5444), 1550–1552.
(4) Lortscher, E.; Ciszek, J. W.; Tour, J.; Riel, H. *Small* **2006**, *2* (8−9), 973–977.
(5) Cai, L. T.; Cabassi, M. A.; Yoon, H.; Cabarcos, O. M.; McGuiness, C. L.; Flatt, A. K.; Allara, D. L.; Tour, J. M.; Mayer, T. S. *Nano Lett.* **2005**, *5* (12), 2365–2372.
(6) Akkerman, H. B.; de Boer, B. *J. Phys.: Condens. Matter* **2008**, *20* (1), No. 013001.
(7) Salomon, A.; Cahen, D.; Lindsay, S.; Tomfohr, J.; Engelkes, V. B.; Frisbie, C. D. *Adv. Mater.* **2003**, *15* (22), 1881–1890.
(8) Venkataraman, L.; Klare, J. E.; Nuckolls, C.; Hybertsen, M. S.; Steigerwald, M. L. *Nature* **2006**, *442* (7105), 904–907.
(9) Troisi, A.; Ratner, M. A. *Small* **2006**, *2* (2), 172–181.
(10) Troisi, A.; Beebe, J. M.; Picraux, L. B.; van Zee, R. D.; Stewart, D. R.; Ratner, M. A.; Kushmerick, J. G. *Proc. Natl. Acad. Sci. U.S.A.* **2007**, *104* (36), 14255–14259.
(11) Galperin, M.; Nitzan, A.; Ratner, M. A. *Phys. Rev. B* **2007**, *76* (3), No. 035301.
(12) Galperin, M.; Nitzan, A.; Ratner, M. A. *Phys. Rev. B* **2006**, *74* (7), No. 075326.
(13) Nie, S. M.; Emery, S. R. *Science* **1997**, *275* (5303), 1102–1106.
(14) Kneipp, K.; Wang, Y.; Kneipp, H.; Perelman, L. T.; Itzkan, I.; Dasari, R.; Feld, M. S. *Phys. Rev. Lett.* **1997**, *78* (9), 1667–1670.
(15) Ward, D. R.; Grady, N. K.; Levin, C. S.; Halas, N. J.; Wu, Y. P.; Nordlander, P.; Natelson, D. *Nano Lett.* **2007**, *7* (5), 1396–1400.
(16) Ioffe, Z.; Shamai, T.; Ophir, A.; Noy, G.; Yutsis, I.; Kfir, K.; Cheshnovsky, O.; Selzer, Y. *Nat. Nanotechnol* **2008**, *3* (12), 727–732.
(17) Martin, C. R. *Science* **1994**, *266* (5193), 1961–1966.
(18) Morrow, T. J.; Li, M. W.; Kim, J.; Mayer, T. S.; Keating, C. D. *Science* **2009**, *323* (5912), 352–352.
(19) Smith, P. A.; Nordquist, C. D.; Jackson, T. N.; Mayer, T. S.; Martin, B. R.; Mbindyo, J.; Mallouk, T. E. *Appl. Phys. Lett.* **2000**, *77* (9), 1399–1401.
(20) Li, M. W.; Bhiladvala, R. B.; Morrow, T. J.; Sioss, J. A.; Lew, K. K.; Redwing, J. M.; Keating, C. D.; Mayer, T. S. *Nat. Nanotechnol.* **2008**, *3* (2), 88–92.

DOI: 10.1021/nl100982q | *Nano Lett.* **2010,** *10,* 2897–2902

(21) Cai, L. T.; Skulason, H.; Kushmerick, J. G.; Pollack, S. K.; Naciri, J.; Shashidhar, R.; Allara, D. L.; Mallouk, T. E.; Mayer, T. S. *J. Phys. Chem. B* **2004**, *108* (9), 2827–2832.
(22) Stapleton, J. J.; Harder, P.; Daniel, T. A.; Reinard, M. D.; Yao, Y. X.; Price, D. W.; Tour, J. M.; Allara, D. L. *Langmuir* **2003**, *19* (20), 8245–8255.
(23) Dequesnes, M.; Rotkin, S. V.; Aluru, N. R. *Nanotechnology* **2002**, *13* (1), 120–131.
(24) Montgomery, S. W.; Franchek, M. A.; Goldschmidt, V. W. *J. Colloid Interface Sci.* **2000**, *227* (2), 567–584.
(25) Lee, T. H.; Wang, W. Y.; Reed, M. A. *Mol. Electron. III* **2003**, *1006*, 21–35.
(26) Adkins, C. J.; Phillips, W. A. *J. Phys. C: Solid State Phys* **1985**, *18* (7), 1313–1346.
(27) Richter, L. J.; Yang, C. S. C.; Wilson, P. T.; Hacker, C. A.; van Zee, R. D.; Stapleton, J. J.; Allara, D. L. *J. Phys. Chem. B* **2004**, *108* (33), 12547–12559.
(28) Kushmerick, J. G.; Allara, D. L.; Mallouk, T. E.; Mayer, T. S. *MRS Bull.* **2004**, *29* (6), 396–402.
(29) Troisi, A.; Ratner, M. A. *J. Chem. Phys.* **2006**, *125* (21), 214709.
(30) Yoon, I.; Kang, T.; Choi, W.; Kim, J.; Yoo, Y.; Joo, S. W.; Park, Q. H.; Ihee, H.; Kim, B. *J. Am. Chem. Soc.* **2009**, *131* (2), 758–762.
(31) Kneipp, K.; Kneipp, H.; Itzkan, I.; Dasari, R. R.; Feld, M. S. *Chem. Phys.* **1999**, *247* (1), 155–162.
(32) Van Duyne, R. P. *Chemical and Biochemical Applications of Lasers*; Academic Press: New York, 1979.
(33) Fromm, D. P.; Sundaramurthy, A.; Kinkhabwala, A.; Schuck, P. J.; Kino, G. S.; Moerner, W. E. *J. Chem. Phys.* **2006**, *124* (6), No. 061101.
(34) Maitani, M. M.; Ohlberg, D. A. A.; Li, Z. Y.; Allara, D. L.; Stewart, D. R.; Williams, R. S. *J. Am. Chem. Soc.* **2009**, *131* (18), 6310–6311.
(35) Xiao, X. Y.; Xu, B. Q.; Tao, N. J. *Nano Lett.* **2004**, *4* (2), 267–271.
(36) Jang, S. Y.; Reddy, P.; Majumdar, A.; Segalman, R. A. *Nano Lett.* **2006**, *6* (10), 2362–2367.

DOI: 10.1021/nl100982q | *Nano Lett.* **2010,** *10,* 2897--2902